IOP Publishing Superconductor Science and Technology
Supercond. Sci. Technol. **33** (2020) 055008 (10pp) https://doi.org/10.1088/1361-6668/ab804b

Coupling time constants and ac loss characteristics of spiral copper-plated striated coated-conductor cables (SCSC cables)

Yusuke Sogabe, Yudai Mizobata and Naoyuki Amemiya

Department of Electrical Engineering, Graduate School of Engineering, Kyoto University, Kyoto-Daigaku-Katsura, Nishikyo, Kyoto 615-8510, Japan

E-mail: amemiya.naoyuki.6a@kyoto-u.ac.jp

Received 12 October 2019, revised 27 February 2020
Accepted for publication 16 March 2020
Published 13 April 2020

Abstract

We conducted electromagnetic field analyses of spiral copper-plated striated coated-conductor cable (SCSC cable), where the striated (multifilament) and copper-plated coated conductors were twisted spirally around a round core in order to decouple the filaments. We used a numerical model which was formulated with current vector potential and in which thin-strip approximation was applied to the superconductor layer of the coated conductors. The nonlinear conductivity obtained from measured electric field–current density characteristics was used to represent the superconducting properties. To confirm the effect of the spiral twist in the SCSC cables, we determined their coupling time constants from the frequency dependences of their calculated magnetisation losses, under an ac transverse magnetic field with a small amplitude. Moreover, we calculated the ac losses in the SCSC cables under simultaneous application of ac transverse magnetic fields and ac transport currents, which represent practical operating conditions for electrical power devices and magnets.

Keywords: ac loss, coated conductor, copper plating, coupling time constant, multifilament, SCSC cable, spiral twist

(Some figures may appear in colour only in the online journal)

1. Introduction

Reducing ac losses and magnetisation in coated conductors will help their application in electrical power devices and magnets. Multifilament structures, in which the superconductor layer of a coated conductor is divided into multiple filaments, is a method to reduce ac losses as well as magnetisation [1–9]. From the viewpoint of improving the robustness of a multifilament coated conductor for local normal transitions, it is preferable to have a finite transverse conductance between the superconductor filaments because it facilitates current sharing between the filaments. When copper is plated over the superconductor filaments to allow current sharing between the filaments, the multifilament structure can effectively reduce ac losses and magnetisation only after the decay of coupling currents flowing through the transverse conductance and the superconductor filaments [10–15]. In particular, if the characteristic time of a time-varying magnetic field and/or a transport current in an actual application is shorter than the decay time constant of the coupling current (coupling time constant), the multifilament structure is ineffective because the superconductor filaments are coupled electromagnetically. Unfortunately, the intrinsic coupling time constant of a flat and straight copper-plated multifilament coated conductor is proportional to the square of its length and generally has a large value [14, 15]. In the case of low T_c metallic superconductors such as Nb–Ti, twisting is a standard technique used to reduce their coupling time constants; however, twisting tape-shaped coated conductors are not practical.

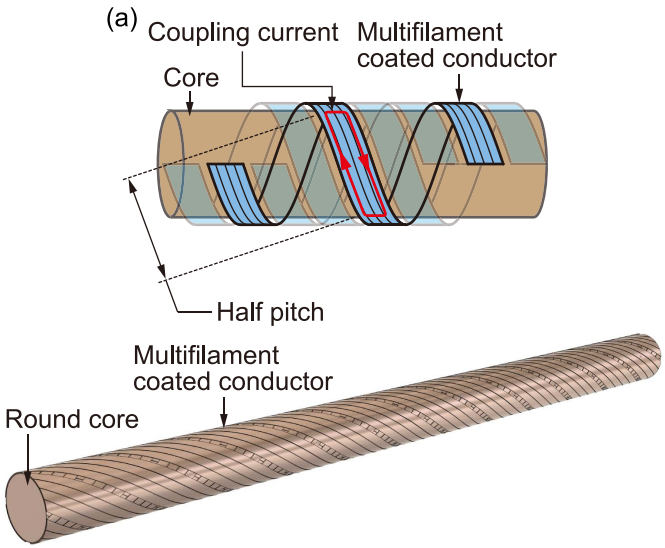

Figure 1. Concept and schematic of SCSC cable: (a) concept of spiral twist in the SCSC cable and confined loop of coupling current in half pitch of the spiral twist and (b) schematic of the SCSC cable.

In this study, we focus on spiral copper-plated striated coated-conductor cables (SCSC cables), where striated (multifilament) and copper-plated coated conductors are twisted spirally around a round core as shown in figure 1 in order to decouple the filaments [16, 17]. The geometry of the SCSC cable is similar to that of the CORC cable [18]. When a transverse magnetic field is applied to this cable, the direction of the magnetic field component normal to the wide face of each multifilament coated conductor varies alternately. Consequently, each loop of the coupling current is confined in a half pitch of the *spiral twist*, as shown in figure 1(a), and the coupling time constant can be reduced substantially. The disadvantage of the SCSC cables as well as the CORC cables is a low engineering current density compared with Roebel cables, which are ones of the most popular assembled coated conductors. However, even if the Roebel cables are composed of copper-plated multifilament coated conductors, it should be noted that the coupling time constants in Roebel cables are not reduced because the strands are not twisted.

Several other groups have studied similar concepts [7, 19, 20], but they used multifilament coated conductors whose superconductor filaments are electrically insulated, and whose electromagnetic behaviours differ from that proposed in this study. For example, there was no concept of the coupling time constant. We have reported proof-of-concept experiments to reduce the coupling time constant via the spiral twist [17]; however, we still need to clarify the electromagnetic behaviours that lead to the reduction of ac loss as well as magnetisation.

The objective of this study is to clarify the electromagnetic behaviours of the SCSC cables through electromagnetic field analyses. First, we conducted the electromagnetic field analyses of the SCSC cables, in which the conductors were exposed to small-amplitude transverse magnetic fields at various frequencies. We determined the coupling time constants from the frequency dependences of the calculated magnetisation losses and discussed the frequency-dependent magnetisation loss with respect to visualised current distributions. Next, we conducted electromagnetic field analyses under more practical conditions (larger field amplitudes and a combination of the transverse magnetic field and the transport current) to demonstrate the reduction of the ac losses in the SCSC cables.

This paper is organised as follows. In section 2, the model for the electromagnetic field analyses is described. In section 3, we determine the coupling time constants of the SCSC cables and discuss them with the visualised current distributions. In section 4, we present the ac loss characteristics as well as the current distributions in the coated conductors under practical operating conditions. Here, we also discuss the frequency dependences of the magnetisation losses in the SCSC cable and reference cables consisting of monofilament coated conductors or insulated multifilament coated conductors. Finally, our conclusions are presented in section 5.

2. Model for electromagnetic field analyses of SCSC cables

2.1. Governing equation of the analyses

From Faraday's law, Bio-Savart's law, Ohm's law and the definition of the current vector potential, we obtainthe governing equation of the electromagnetic field analyses as follows:

$$\nabla \times \left(\frac{1}{\sigma} \nabla \times \boldsymbol{T} \right) + \frac{\partial}{\partial t} \frac{\mu_0}{4\pi} \int_V \frac{(\nabla \times \boldsymbol{T'}) \times \boldsymbol{r}}{r^3} \mathrm{d}V = 0. \quad (1)$$

Thin-strip approximation was applied to our analysis model. Electromagnetic field analyses via the finite element method were conducted, based on the following equation [21]:

$$\nabla \times \left(\frac{1}{\sigma} \nabla \times \mathbf{n} T \right) \cdot \mathbf{n} + \frac{\partial}{\partial t} \frac{\mu_0 t_s}{4\pi} \int_{S'} \frac{(\nabla \times \mathbf{n}' T') \times \boldsymbol{r} \cdot \boldsymbol{n}}{r^3} \mathrm{d}S' = 0. \quad (2)$$

Here, T and T' are the magnitudes of current vector potential at the point where the field (potential) was calculated (the field point) and the point where the current was flowing (the source point), respectively; $\boldsymbol{n}$ and $\boldsymbol{n}'$ are the normal vectors at the field point and the source point, respectively; $\boldsymbol{r}$ is the vector from the source point to the field point, and r is its length; t_s is the thickness of the superconductor layer of the coated conductor. In the analyses of the multifilament coated conductors plated with copper, σ indicates equivalent conductivity of the superconductor filaments or the conductivity of a narrow normal conducting strip (details are described in section 2.3).

2.2. Equivalent conductivity of superconductor layer

The conductivity of the superconductor layer in coated conductors was formulated from the measured electric field E–current density J characteristics of a coated conductor. It should be noted that we have to consider the dependence on

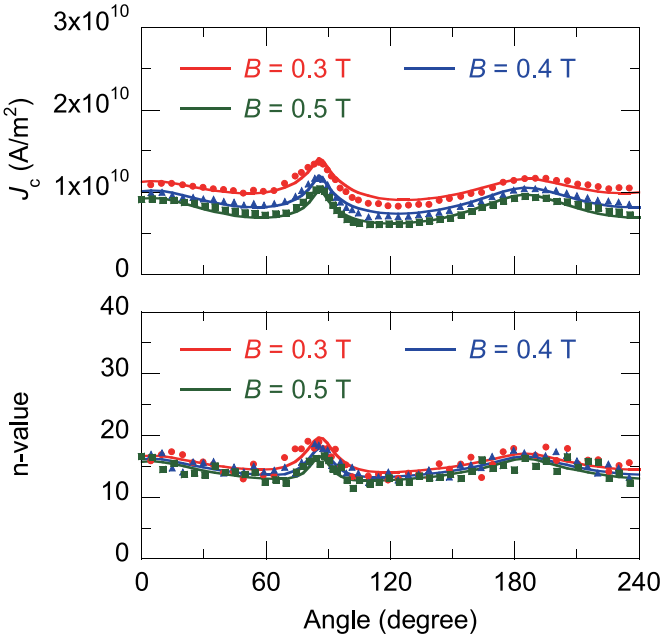

Figure 2. Dependence of critical current density J_c and n-value in the power-law model on magnitude of magnetic flux density B and its orientation φ at temperature $T = 77$ K.

the magnitude of magnetic field B, its orientation φ, and temperature T. We used the power-law model for the analyses at 77 K and the percolation depinning model for the analyses at 30 K. The parameters of both models were derived from the measured E–J characteristics of an actual coated conductor. We primarily focused on coupling time constants. On this account, it should be noted that coupling time constants are independent of E–J characteristics. However, in order to calculate the entire losses of cables, we needed the E–J characteristics which depend on B and φ.

The power-law model is described as follows:

$$E = E_0 (J/J_c(B,\phi))^{n(B,\phi)}, \tag{3}$$

where E_0 is a criterion electric field to define critical current density J_c and is set at 1×10^{-4} V m^{-1}. In this model, both J_c and the n-value are dependent on B and φ. The formulation of the dependences of J_c and the n-value on B and φ is described in detail in [22]. We used the E–J characteristics measured at 77 K, and the fitted results are shown in figure 2 and table 1.

In the percolation depinning model [23–26], E is given as:

$$E = \begin{cases} 0 & \text{for } J < J_{cm} \\ \frac{\rho_{FF} J_0}{m+1} \left(\frac{J - J_{cm}}{J_0} \right)^{m+1} & \text{for } J_{cm} \geqslant 0 \\ \frac{\rho_{FF} J_0}{m+1} \left[\left(\frac{J + |J_{cm}|}{J_0} \right)^{m+1} - \left(\frac{|J_{cm}|}{J_0} \right)^{m+1} \right] & \text{for } J_{cm} < 0 \end{cases}, \tag{4}$$

where ρ_{FF} and m are parameters. J_0 and J_{cm} satisfy following equations;

$$F_{pm} = J_{cm} B \tag{5}$$

$$F_{pk} = (J_{cm} + J_0) B, \tag{6}$$

where

$$F_{pm(pk)} = \begin{cases} A B_{GL(k)}(T,0)^{\zeta} f(\phi)^{\hat{\zeta}} \left(\frac{B}{B_{GL(k)}(T,\phi)} \right)^{\gamma} \left(1 - \frac{B}{B_{GL(k)}(T,\phi)} \right)^{\delta} & \text{for } B \leqslant B_{GL(k)}(T,\phi) \\ -A B_{GL(k)}(T,0)^{\zeta} f(\phi)^{\hat{\zeta}} \left| 1 - \frac{B}{B_{GL(k)}(T,\phi)} \right|^{\delta} & \text{for } B > B_{GL(k)}(T,\phi) \end{cases}. \tag{7}$$

Here, the subscripts pm(pk) and GL(k) means pm or pk and GL or k, respectively. The values of the parameters A, ζ, $\hat{\zeta}$, γ, and δ for F_{pm} and those for F_k have different values. $B_{GL(k)}$ are given as

$$B_{GL(k)}(T,0) = \frac{b}{1-\nu_p} \left(1 - \frac{T}{T_c} \right) \left\{ 1 - \frac{a}{1 - T/T_c} + \sqrt{\left(1 + \frac{a}{1 - T/T_c} \right)^2 - 4\nu_p \frac{a}{1 - T/T_c}} \right\}, \tag{8}$$

$$B_{GL(k)}(T,\phi) = B_{GL(k)}(T,0) f(\phi). \tag{9}$$

Here, equation (8) describes the temperature dependence of $B_{GL(k)}$. The values of a, b, and ν_p for B_{GL} and those for B_k are different. T_c is the critical temperature of the superconductor. We consider two different pinning centres in the superconductor: the ab surface pin and c axis pin. In this case, E corresponding to a specific J is calculated by using equations (4)–(9) and the parameters for each pin (i.e. E_{ab} and E_c). Then, we choose a smaller value of E as the electric field in the superconductor. For each pin, $f(\varphi)$ is defined as follows:

$$f(\phi) = \begin{cases} \frac{1}{\sqrt{\cos^2\phi + \alpha^2 \sin^2\phi}} & \text{for ab surface pin} \\ \frac{1}{\sqrt{\alpha^2 \cos^2\phi + \sin^2\phi}} & \text{for } c \text{ axis pin} \end{cases}. \tag{10}$$

The above equations were fitted to the E–J characteristics of a coated conductor measured at 30 K to determine the parameters. The obtained parameters are listed in table 2, and the fitted E–J curves are shown in figure 3.

Table 1. Parameters of fitting results of dependences of J_c and n-value at $T = 77$ K.

Fitting parameters for formulation of J_c		Fitting parameters for formulation of n-value	
m	0.0966	m	1.26
J_{c0ab}	0.402	n_{0ab}	14.5
$J_{c0\ c}$	9.39×10^9	$n_{0\ c}$	19.1
B_{0ab}	3.38	B_{0ab}	9.73×10^6
$B_{0\ c}$	3.29	$B_{0\ c}$	0.368
β_{ab}	6.87	β_{ab}	1.61×10^7
β_c	2.07	β_c	0.218
u_{ab}	42.0	u_{ab}	13.2
u_c	3.51	u_c	4.33
v	0.845	v	0.811
δ_{ab}	–4°	δ_{ab}	–4°
δ_c	5°	δ_c	5°

Table 2. Parameters of the percolation depinning model at $T = 30$ K.

Parameters	*ab* surface pin	*c* axis pin
T_c	92.5	92.5
m	2.52	3.83
ρ_{FF}	1.00×10^{-7}	1.00×10^{-7}
α	2.37	229
F_{pm}/F_{pk}		
A	$1.88 \times 10^9/5.00 \times 10^{10}$	$1.74 \times 10^9/2.27 \times 10^9$
ζ	1.33/1.36	1.87/1.68
$\hat{\zeta}$	0.938/1.10	1.55/0.435
γ	0.436/0.294	1.58/0.851
δ	2.47/2.50	0.780/2.83
B_{GL}/B_k		
a	1.00/1.00	1.00/1.00
b	30.2/23.4	83.7/40.2
ν_p	0.954/0.977	0.956/0.971

2.3. Modelling of the transverse conductance between superconductor filaments

When we conducted the electromagnetic field analyses of copper-plated multifilament coated conductors, the thin-strip approximation was applied, as described in section 2.1. Although the transverse conductance between the superconductor filaments can consist of the plated copper in actual conductors, it was modelled as the thin strip of a normal conductor. The normal conducting thin strips had the same thickness as that of the superconductor filaments t_s in equation (2). The conductivity of the normal conducting thin strips was determined by measuring coupling time constants of straight copper-plated multifilament coated conductors at 77 K [14] compensating for the difference in the thickness of the model from the actual thickness of the plated copper in the measured samples. Additionally, to determine the conductivity of the normal conducting thin strips at 30 K, a formulated temperature dependence of the conductivity of copper [27] was considered.

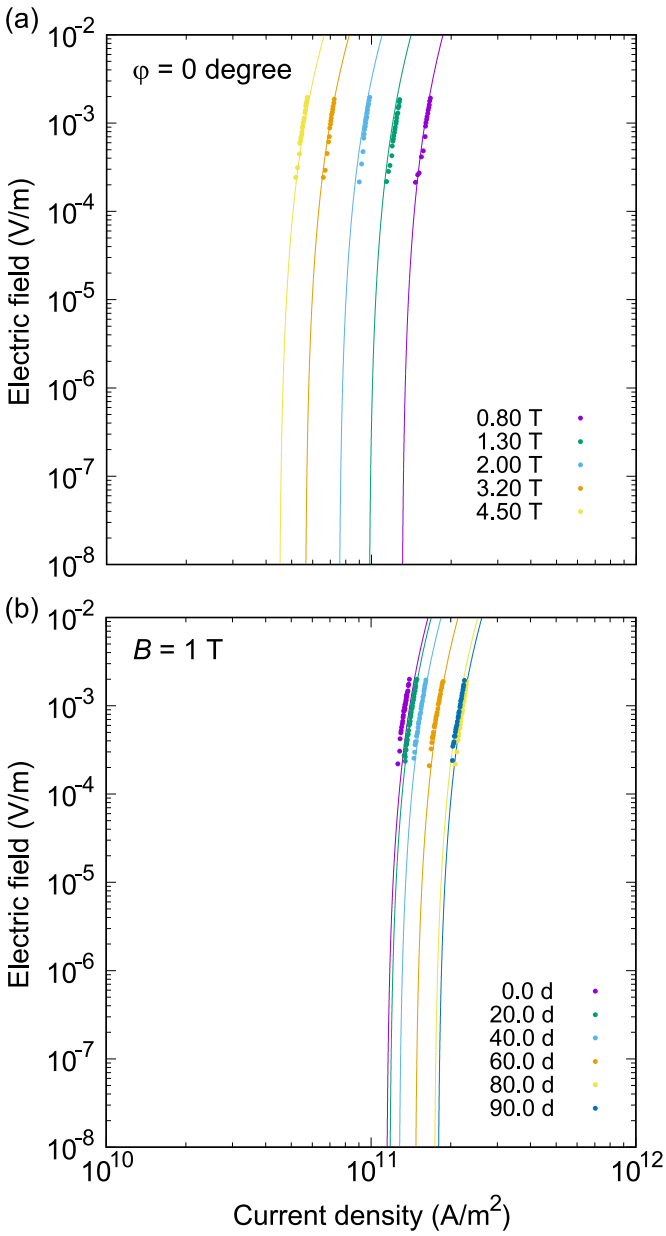

Figure 3. Fitted electric field E–current density J characteristics by the percolation depinning model: (a) dependence on B with $\varphi = 0°$ and (b) dependence on φ with $B = 1$ T.

2.4. Specifications of SCSC cables and reference cables

In our model, we considered the three-dimensional geometry of the SCSC cables and reference cables. The detailed specifications of the analysed SCSC cables and the reference cables are listed in table 3. The reference cables have similar geometries to the SCSC cables but consist of monofilament coated conductors (Ref-MN cables) or insulated multifilament coated conductors (Ref-INS cables). In the multilayer SCSC cables and reference cables, coated conductors were twisted alternately in right-hand-thread and left-hand-thread directions layer-by-layer. The conductors in the innermost layer were twisted in the right-hand-thread direction; the odd-numbered layers overlapped completely with each

Table 3. Specifications of SCSC cable and reference cables.

Cable name	SCSC cable	Ref-MN cable	Ref-INS cable
	Coated conductors		
Number of superconductor filaments	4	1	4
Gap between superconductor filaments	50 μm Conducting	None	50 μm Insulating
Width of coated conductor	3 mm	3 mm	3 mm
Thickness of coated conductor	45 μm	45 μm	45 μm
Thickness of superconductor layer t_s	1.6 μm	1.6 μm	1.6 μm
Thickness of plated copper	20 μm	20 μm	20 μm
	Cable geometry		
Diameter of core	2.7 mm		
Number of coated conductors per layer	2		
Number of layers	1/2/4		
Pitch of spiral	10 mm		
Direction of spiral	The innermost layer: right-hand-thread direction Other layers: alternative direction		
Separation between coated conductors in adjacent layers	0 mm		

other, and the even-numbered layers were spirally twisted similarly.

In the analyses, we reduced the analysed regions by using their geometrical symmetries [21]. As we could assume the same current density distribution in the coated conductors in the same layer, the analysed region could be reduced to one coated conductor per layer. Furthermore, as the same current density distributions could be repeated for every pitch length, a single pitch length was sufficient for the analyses. Note that we considered a sufficient length of the cables with the same current density distributions in the corresponding analysed region to calculate self-fields by transport current in infinitely long cables.

3. Coupling time constants of SCSC cables

3.1. Method to determine coupling time constants

To estimate the coupling time constants τ_c, we conducted the electromagnetic field analyses of the SCSC cables exposed to a sinusoidal transverse magnetic field with small amplitude and various frequencies f. When we plot the magnetisation losses dominated by coupling losses with respect to the frequency and obtain the curve against frequency with peak f_c, the coupling time constant τ_c is given by the following expression [14, 28, 29]:

$$\tau_c = 1/2\pi f_c. \tag{11}$$

3.2. Coupling time constant of single-layer SCSC cable

Firstly, we analyse the SCSC cable whose number of layer n_l was one where the amplitude of the transverse magnetic field $\mu_0 H_m$ was 1 mT. Figure 4 shows the frequency dependence of the calculated magnetisation losses where the peak of the curve appears at $f_c = 4979$ Hz. Therefore, the coupling time constant was calculated as 0.032 ms by using equation (11).

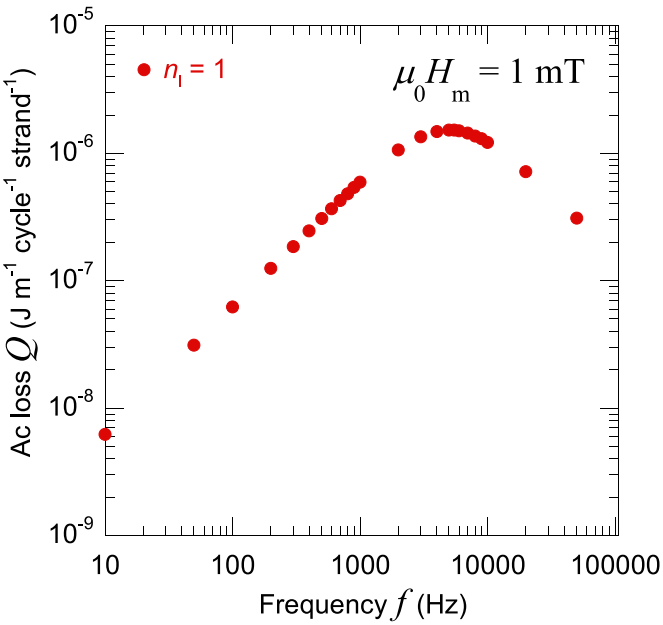

Figure 4. Dependence of magnetisation loss of the 1-layer SCSC cable on frequency f at applied transverse magnetic field at $\mu_0 H_m = 1$ mT and $T = 77$ K.

This coupling time constant is sufficiently smaller than the characteristic times of the changes in the magnetic fields or the transport currents in actual applications.

Figure 5 depicts the current lines in the half pitch of the SCSC cable at three frequencies: 500 Hz ($\sim f_c/10$), 5 kHz ($\sim f_c$), and 50 kHz ($\sim 10 f_c$). It should be noted that all loops of the currents, including shielding/coupling currents, are confined in the half pitch. This is the effect of the spiral twist. When frequency f was 500 Hz (figure 5(a)), because the frequency was much lower than f_c, the induced shielding currents were confined in the filaments and the coupling currents did

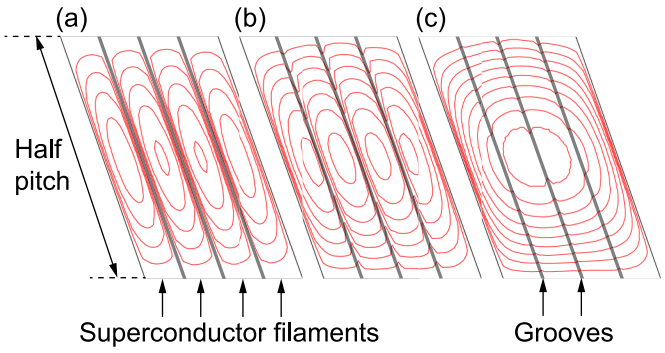

Figure 5. Current lines in half pitch of the 1-layer SCSC cable at $\mu_0 H_m = 1$ mT and $T = 77$ K; (a) $f = 500$ Hz, (b) $f = 5$ kHz and (c) $f = 50$ kHz. Current lines are plotted within 0.2 A line^{-1}.

not flow among the filaments. Notably, in this case, the superconductor filaments were electromagnetically decoupled. In contrast, when frequency f was 50 kHz (figure 5(c)), because the frequency was much higher than f_c, we could see the coupling currents flowing among the filaments. In other words, the superconductor filaments were electromagnetically coupled. Because the current lines at $f = 5$ kHz shown in figure 5(b) were intermediate between those at $f = 500$ Hz and those at $f = 50$ kHz, we could see both the coupling currents flowing among filaments and the shielding currents confined in the filaments.

3.3. *Influence of number of layers on coupling time constant*

Under a 1 mT sinusoidal transverse magnetic field, the magnetisation losses were calculated for SCSC cables with various n_l at $T = 77$ K and $T = 30$ K. The frequency dependences of the magnetisation losses at $T = 77$ K and $T = 30$ K are shown in figures 6(a) and (b), respectively. The magnetisation losses in the analysed coated conductors with larger n_l were slightly smaller due to the stronger diamagnetic field effect caused by stacking coated conductors in the cables.

The obtained coupling time constants for all cases are listed in table 4. The coupling time constants at $T = 30$ K were higher than that at $T = 77$ K due to higher transverse conductivity at lower temperatures. Additionally, the coupling time constants were almost independent of n_l at both temperatures. This indicates that an increasing number of layers does not deteriorate the decoupling effect of the spiral twist whereas it increases the current carrying capacity.

4. AC losses in SCSC cables under practical conditions

4.1. *Conditions of analyses*

To estimate the effect of the spiral twist and the multifilament structures on ac loss reduction, we conducted the electromagnetic field analyses of the SCSC cables and the reference cables under practical operating conditions. Here, we set four typical conditions.

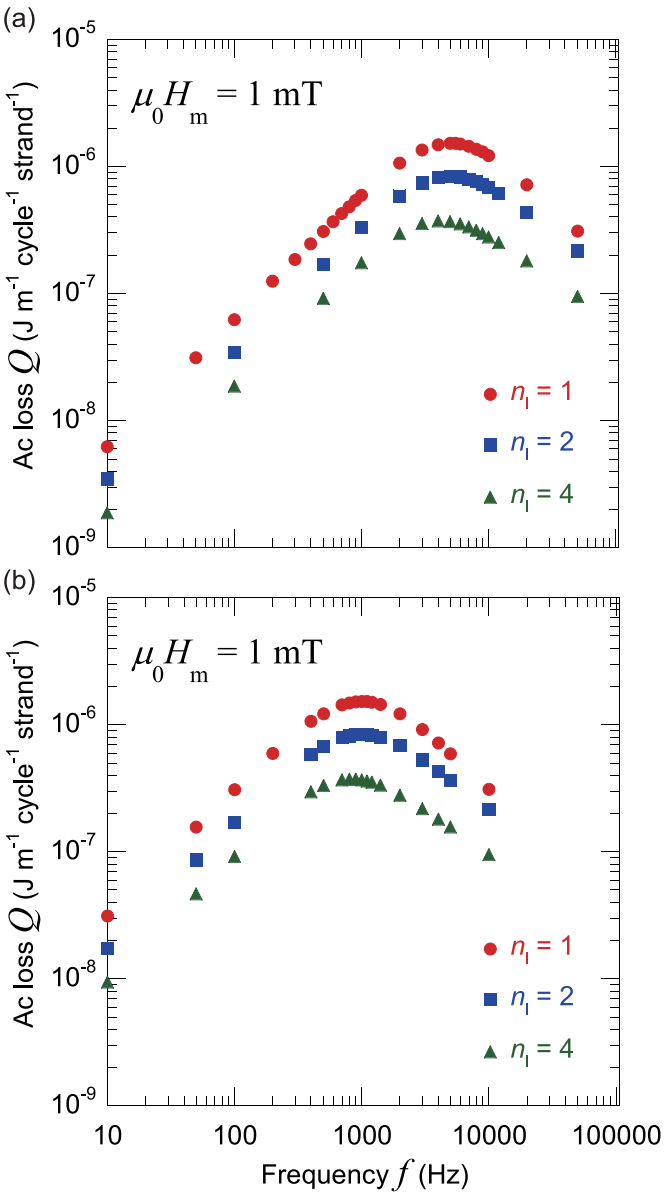

Figure 6. Magnetisation loss of the SCSC cables with different number of layers n_l with respect to frequency at $\mu_0 H_m = 1$ mT; (a) $T = 77$ K and (b) $T = 30$ K.

Condition 1A: The cables were only exposed to a sinusoidal transverse magnetic field with $\mu_0 H_m = 0.3$ T and frequency $f = 50$ Hz.

Condition 1B: The cables were exposed to a sinusoidal transverse magnetic field ($\mu_0 H_m = 0.3$ T) and were carrying a sinusoidal transport current whose amplitude per coated conductor I_t was 30 A. The transverse magnetic field and the transport current were in the coordinate phase, and their frequency was 50 Hz.

These conditions simulate actual operating conditions of power applications such as transformers and armature winding of rotating machines.

Condition 2A: The cables were only exposed to a triangular transverse magnetic field with $\mu_0 H_m = 3$ T and $f = 0.5$ Hz. Here, the triangular transverse magnetic field was formulated

Table 4. Peak frequencies and coupling time constants of the SCSC cables with different number of layers at 77 K and 30 K.

$T = 77$ K		
Number of layers	Peak frequencies	Coupling time constants
1	4.98 kHz	32.0 μs
2	5.12 kHz	31.1 μs
4	4.36 kHz	36.5 μs
$T = 30$ K		
Number of layers	Peak frequencies	Coupling time constants
1	1.00 kHz	159 μs
2	1.04 kHz	153 μs
4	0.89 kHz	177 μs

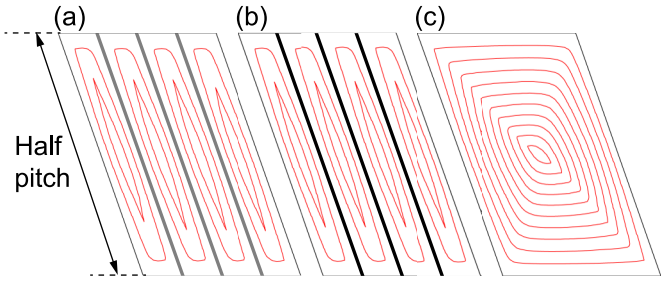

Figure 7. Current lines in half pitch of the 1-layer SCSC cable and the 1-layer reference cables exposed to a sinusoidal transverse magnetic field whose $\mu_0 H_m$ is 0.3 T, and f is 50 Hz, and $T = 77$ K: (a) SCSC cable, (b) Ref-INS cable, and (c) Ref-MN cable. The current lines are plotted when the transverse field is at peak with 8 A per line.

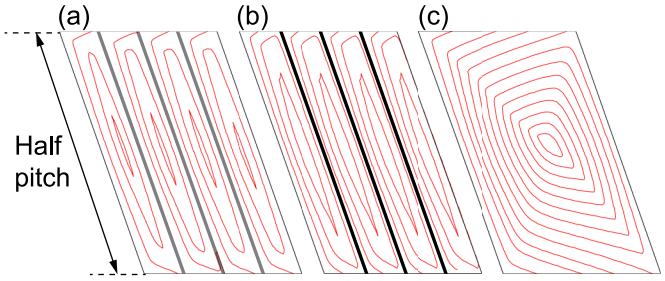

Figure 8. Current lines in half pitch of the 1-layer SCSC cable and the 1-layer reference cables exposed to a sinusoidal transverse magnetic field whose $\mu_0 H_m$ is 0.3 T and carrying sinusoidal transport current whose amplitude per coated conductor I_t is 30 A at $T = 77$ K. The magnetic field and the transport current are in phase, and f is 50 Hz: (a) SCSC cable, (b) Ref-INS cable, and (c) Ref-MN cable. The current lines are plotted when the transverse field and the transport current is at peak with 7.5 A per line.

as follows:

$$t = \tau + k/f \quad (k: \text{integer}, 0 \le \tau < 1/f)$$

$$\mu_0 H(\tau) = \begin{cases} \mu_0 H_m \cdot 2f \cdot \tau & \text{when } 0 \le \tau \le 1/2f \\ 2\mu_0 H_m - \mu_0 H_m \cdot 2f \cdot \tau & \text{else} \end{cases}. \quad (12)$$

Condition 2B: The cables were exposed to a triangular transverse magnetic field ($\mu_0 H_m = 3$ T) and were carrying a triangular transport current ($I_t = 150$ A). The transverse magnetic field and transport current were in the coordinate phase, and their frequency was 0.5 Hz.

These conditions simulate the actual operating conditions of fast ramped magnets operated under a medium field.

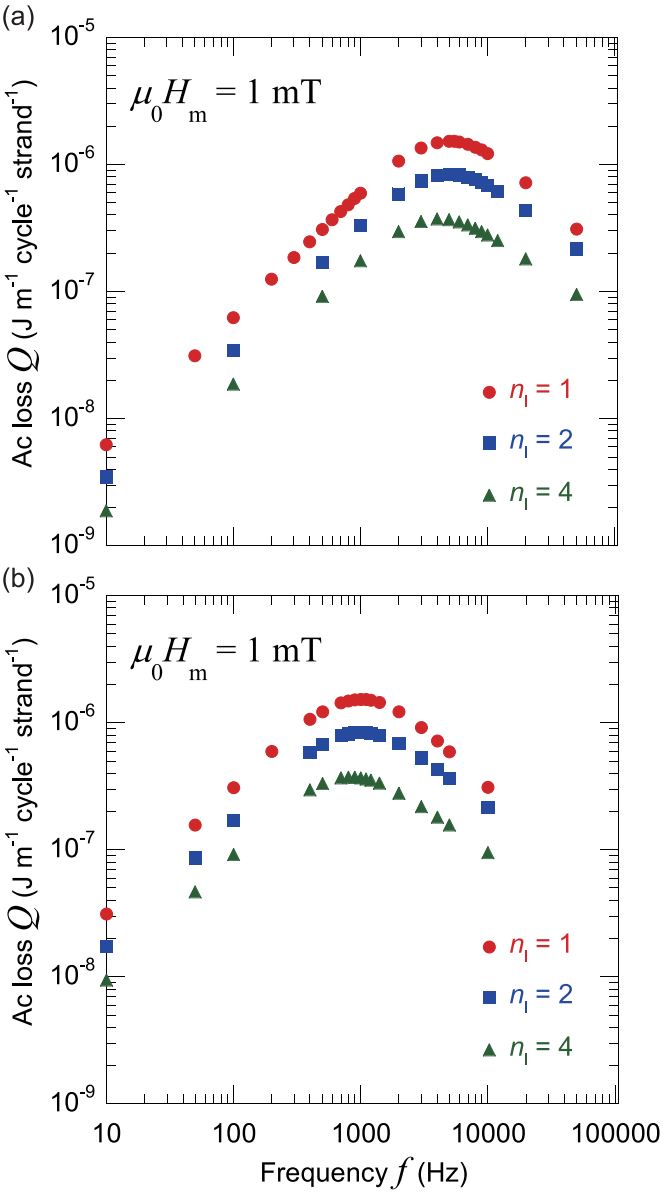

Figure 9. Ac losses of the SCSC cables and the reference cables with different n_l at $T = 77$ K: (a) a sinusoidal transverse magnetic field with $\mu_0 H_m = 0.3$ T and $f = 50$ Hz and (b) a sinusoidal transverse magnetic field with $\mu_0 H_m = 0.3$ T and $f = 50$ Hz and a sinusoidal transport current with $I_t = 30$ A which is in phase with sinusoidal transverse magnetic field. In (a), the ac losses calculated by Brandt's equation is also plotted for a monofilament coated conductor and insulated 4-filament coated conductor.

4.2. Calculated ac losses and current distributions in SCSC cables and reference cables

Figure 7(a) depicts the current lines in the half pitch length of the coated conductor of the SCSC cable under Condition 1A. As a comparison, figures 7(b) and (c) present the current

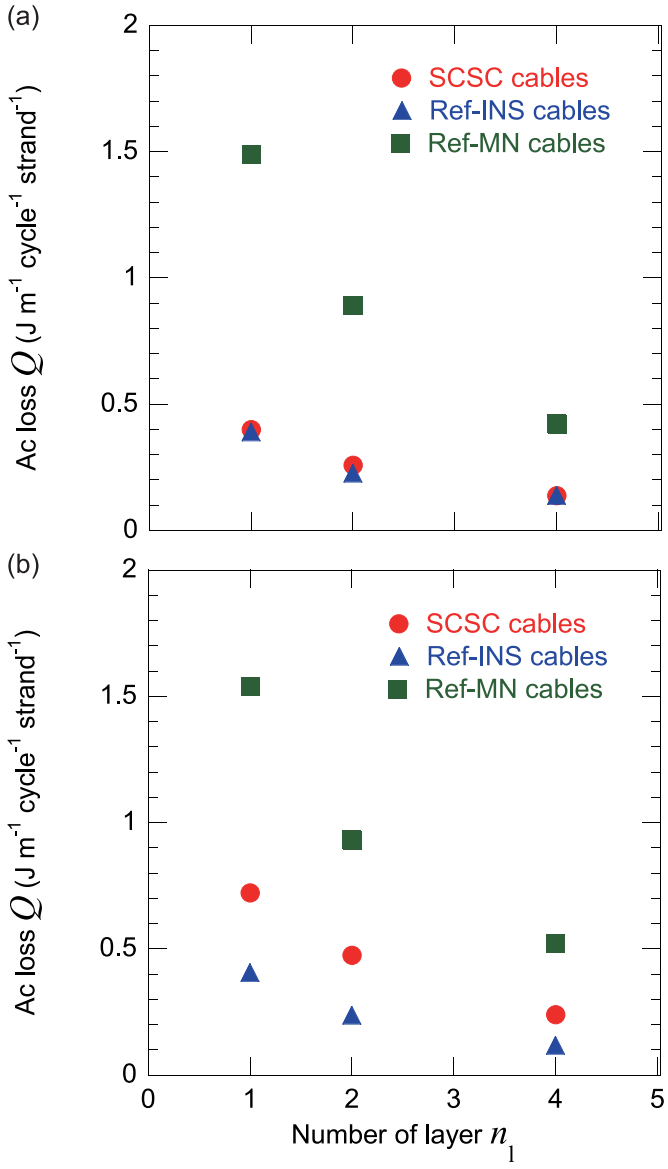

Figure 10. Ac losses of the SCSC cables and the reference cables with different n_l at $T = 30$ K: (a) a triangular transverse magnetic field with $\mu_0 H_m = 3$ T and $f = 0.5$ Hz and (b) a triangular transverse magnetic field with $\mu_0 H_m = 3$ T and $f = 0.5$ Hz and a triangular transport current with $I_t = 150$ A which is in phase with triangular transverse magnetic field.

lines in the half pitch length of the coated conductor of the Ref-INS cable and Ref-MN cable, respectively. Here, n_l was one for the analysed cables and the current lines were plotted at the peak of the transverse magnetic field. There was almost no difference between the current lines in the SCSC cable and those in the Ref-INS cable. This was because the coupling time constant was independent of the amplitude of the transverse magnetic field, and 50 Hz is a significantly lower frequency than the value of f_c in section 3.2. The current lines in the coated conductor in each cable under Condition 1B are shown in figure 8. In this case, the current lines in the SCSC cable were similar to those in the Ref-INS cable.

The ac losses per coated conductor under Conditions 1A and 1B in the cables with different n_l are shown in figures 9(a) and (b), respectively. To compare the analytical solutions of ac losses in spiral-twisted coated conductors with the calculation results, we use Brandt's equation [30]. From Brandt's equation, the hysteresis loss per length per cycle of single superconductor strip, Q_{Brandt}, under a normal magnetic field is described as follows:

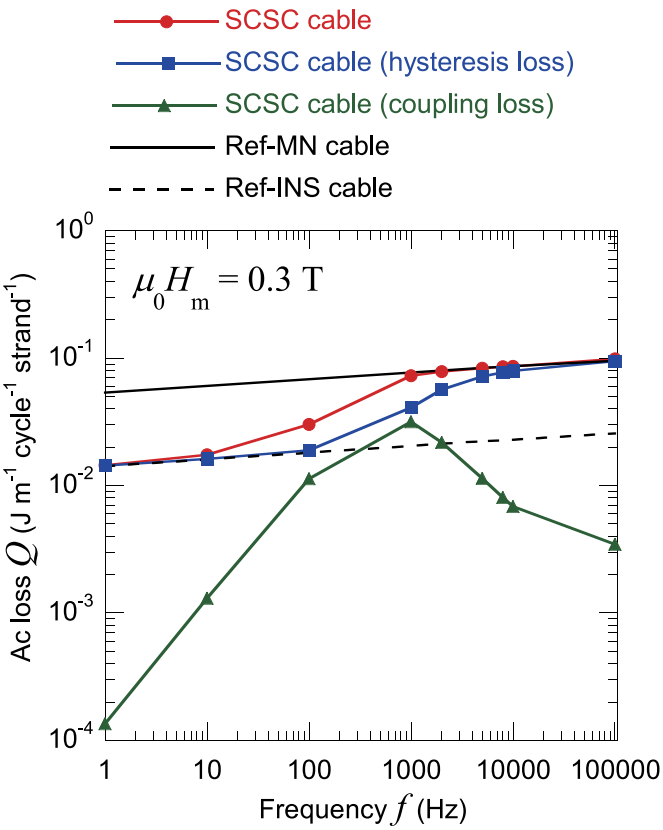

Figure 11. Dependences of the hysteresis loss and the coupling loss of the SCSC cable on f under sinusoidal transverse magnetic field with $\mu_0 H_m = 0.3$ T and $T = 77$ K plotted with the overall ac losses of the SCSC cable, Ref-MN cable, and Ref-INS cable. Every cable was with $n_l = 1$.

$$Q_{Brandt} = \mu_0 w I_c H_{ext} \cdot g\left(\frac{H_{ext}}{H_c}\right). \tag{13}$$

Here, w and I_c are the width and the critical current of the strip, respectively. H_{ext} is the amplitude of the external magnetic field. H_c is calculated as $H_c = I_c/w\pi$ and $g(x)$ is a function given as follows:

$$g(x) = (2/x)\ln(\cosh(x)) - \tanh(x). \tag{14}$$

To use the equation for spiral-twisted coated conductors, we consider weighted average of Q_{Brandt} against φ as follows:

$$Q_{Brandt,spiral} = \int_0^{2\pi} Q_{Brandt}(\phi)\,d\phi/2\pi = \frac{2}{\pi} Q_{Brandt}. \tag{15}$$

In figure 9(a), $Q_{Brandt,spiral}$ is plotted for a monofilament coated conductor (MN) and insulated 4-filament coated conductor (INS) as a reference. In the calculation, we use critical currents under self-field condition which are 120 A for MN

and 30 A for each filament of INS as I_c in (13). The ac losses in the Ref-INS cables are smaller than those in the Ref-MN cables under both conditions because of the effect of the spiral twist and the multifilament. The ac losses in the SCSC cables were almost identical to those in the Ref-INS cables due to the electrical decoupling. From the results, we confirmed that the SCSC cables were effective in reducing the ac losses as well as the magnetisation under the practical conditions simulating power applications.

Figures 10(a) and (b) showed the ac losses per coated conductor in the cables with different n_l under Conditions 2A and 2B, respectively. The ac losses in the Ref-INS cables are also significantly smaller than those in the Ref-MN cables under the conditions. When the SCSC cables carried a transport current, the effect of the multifilament coated conductor on the reduction of the ac losses was slightly deteriorated. However, we can also obtain a satisfactory reduction of ac losses and magnetisation by the multifilament under these practical conditions simulating magnet applications.

4.3. Frequency dependence of ac loss components in spiral coated conductor cables

In this section, we discuss the characteristics of components of the ac losses in the SCSC cables. The ac losses in the SCSC cables can be separated into two components: hysteresis loss and coupling loss. The hysteresis loss is generated in the superconductor filaments, and the coupling loss is generated in the normal conducting thin-strip between the superconductor filaments.

The components of the ac loss in the SCSC cable were plotted with respect to frequency, as shown in figure 11, with the overall ac loss in the SCSC cable as well as that of the Ref-MN cable and that of the Ref-INS cable. Here, the cables were only exposed to a sinusoidal transverse magnetic field whose amplitude $\mu_0 H_m$ was 0.3 T and n_l for each cable was one. In the low-frequency region, because the coupling loss is significantly small, the overall ac loss of the SCSC cable was almost the same as that of the Ref-INS cable. In the medium frequency region (near to f_c), the hysteresis loss and the coupling loss increased and the overall ac loss of the SCSC cable approaches that of the Ref-MN cable. In the high-frequency region, the overall ac loss of the SCSC cable was approximately equal to that of the Ref-MN cable, even though the coupling loss was reduced.

5. Conclusion

In spiral copper-plated striated coated-conductor cables (SCSC cables), the coupling current is confined to a half pitch of the spiral twist. Because the coupling time constant is proportional to the square of the length of the coupling-current loop, the spiral twist is effective in reducing the coupling time constant. The coupling time constants obtained from the frequency dependences of the calculated magnetisation losses were smaller than the characteristic times of the magnetic field and/or the transport current changes in practical applications. Moreover, the coupling time constants are almost independent of the number of layers of the SCSC cables. Therefore, we can increase the current carrying capacity by increasing the number of layers, simultaneously limiting ac loss and magnetisation with the spiral twist.

Through electromagnetic field analyses under practical operating conditions, such as the field/current amplitudes and the frequencies, the effect of the spiral twist in the SCSC cable was confirmed. The ac losses were smaller than those in the reference cables consisting of monofilament coated conductors (Ref-MN cables) and almost same as those in the reference cables consisting of insulated multifilament coated conductors (Ref-INS cables). Further reduction of the ac loss could be achieved by using 100- or 1000-filament coated conductors. However, unfortunately, 100- or 1000-filament coated conductors are not practical because of their present fabrication process. The effect of the spiral twist in the SCSC cable was also confirmed by comparing the frequency dependence of the magnetisation loss in a SCSC cable with that in a Ref-MN cable and that in a Ref-INS cable.

Acknowledgment

This work was supported in part by JST-Mirai Program Grant Number JPMJMI19E1, Japan.

ORCID iDs

Yusuke Sogabe https://orcid.org/0000-0003-1692-629X
Naoyuki Amemiya https://orcid.org/0000-0002-3000-864X

References

[1] Grilli F and Kario A 2016 How filaments can reduce AC losses in HTS coated conductors: a review *Supercond. Sci. Technol.* **29** 083002
[2] Carr W J Jr and Oberly C E 1999 Filamentary YBCO conductors for AC applications *IEEE Trans. Appl. Supercond.* **9** 1475–8
[3] Cobb C B, Barnes P N, Haugan T J, Tolliver J, Lee E, Sumption M, Collings E and Oberly C E 2002 Hysteretic loss reduction in striated YBCO *Physica* C **382** 52–56
[4] Amemiya N, Kasai S, Yoda K, Jiang Z, Levin G A, Barnes P N and Oberly C E 2004 AC loss reduction of YBCO coated conductors by multifilamentary structure *Supercond. Sci. Technol.* **17** 1464–71
[5] Sumption M, Collings E and Barnes P 2005 AC loss in striped (filamentary) YBCO coated conductors leading to designs for high frequencies and field-sweep amplitudes *Supercond. Sci. Technol.* **18** 122–34
[6] Barnes P N, Levin G, Varanasi C and Sumption M D 2005 Low AC loss structures in YBCO coated conductors with filamentary current sharing *IEEE Trans. Appl. Supercond.* **15** 2827–30
[7] Šouc J, Gömöry F, Kováč J, Nast R, Jung A, Vojenčiak M, Grilli F and Goldacker W 2013 Low AC loss cable produced from transposed striated CC tapes *Supercond. Sci. Technol.* **26** 075020
[8] Vojenčiak M, Kario A, Ringsdorf B, Nast R, van der Laan D C, Scheiter J, Jung A, Runtsch B,

Gömöry F and Goldacker W 2015 Magnetization AC loss reduction in HTS CORC® cables made of striated coated conductors *Supercond. Sci. Technol.* **28** 104006

[9] Pardo E, Kapolka M, Kováč J, Šouc J, Grilli F and Piqué R N A 2016 Three-dimensional modeling and measurement of coupling AC loss in soldered tapes and striated coated conductors *IEEE Trans. Appl. Supercond.* **26** 4700607

[10] Levin G A, Barnes P N, Amemiya N, Kasai S, Yoda K and Jiang Z 2005 Magnetization losses in multifilament coated superconductors *Appl. Phys. Lett.* **86** 072509

[11] Kasai S and Amemiya N 2005 Numerical analysis of magnetization loss in finite-length multifilamentary YBCO coated conducotrs *IEEE Trans. Appl. Supercond.* **15** 2855–8

[12] Yanagisawa Y, Xu Y, Jin X, Nakagome H and Maeda H 2015 Reduction of screening current-induced magnetic field of REBCO coils by the use of multi-filamentary tapes *IEEE Trans. Appl. Supercond.* **25** 6603705

[13] Fujita S *et al* 2017 Characterization of multifilamentary REBCO coated conducotr coil fabricated by using the process of scratching the IBAD-MgO layer *IEEE Trans. Appl. Supercond.* **27** 6600504

[14] Amemiya N, Tominaga N, Toyomoto R, Nishimoto T, Sogabe Y, Yamano S and Sakamoto H 2018 Coupling time constants of striated and copper-plated coated conductors and the potential of striation to reduce shielding-current-induced fields in pancake coils *Supercond. Sci. Technol.* **31** 025007

[15] Amemiya N, Sogabe Y, Yamano S and Sakamoto S 2019 Shielding current in a copper-plated multifilament coated conductor wound into a single pancake coil and exposed to a normal magnetic field *Supercond. Sci. Technol.* **32** 115008

[16] Yan Y, Qu T, Zhang Z, Wu Q, Shi Z and Song M 2019 Numerical study on the coupling current and magnetization loss of striated CORC cables using 3D T-A formulation *26th Int. Conf. on Magnet Technology* (Vancouver, Canada, September 2019) *IEEE Trans. Appl. Supercond.* **30** 4800305

[17] Li Y, Inoue S, Kim D H, Amemiya N, Yoshida Y and Machi T 2019. Coupling time constants measurements of spirally wound striated coated conductors *26th Int. Conf. on Magnet Technology* (Vancouver, Canada, September 2019) *IEEE Trans. Appl. Supercond.* **30** 4700905

[18] van der Laan D C, Noyes P D, Miller G E, Weijers H W and Willering G P 2013 Characterization of a high-temperature superconducting conductor on round core cables in magnetic fields up to 20 T *Supercond. Sci. Technol.* **26** 045005

[19] Lee J K, Kim Y, Lee S, Kim W S, Park S H, Park C and Choi K 2013 AC loss analysis of striated HTS compact cables for low loss cable design *IEEE Trans. Appl. Supercond.* **23** 5900804

[20] Vojenčiak M, Kario A, Ringsdorf B, Nast R, van der Laan D C, Scheiter J, Jung A, Runtsch B, Gömöry F and Goldacker W 2015 Magnetization ac loss reduction in HTS CORC® cables made of striated coated conductors *Supercond. Sci. Technol.* **28** 104006

[21] Nii M, Amemiya N and Nakamura T 2012 Three-dimensional model for numerical electromagnetic field analyses of coated superconductors and its application to Roebel cables *Supercond. Sci. Technol.* **25** 095011

[22] Sogabe Y, Jiang Z, Wimbush S C, Stricland N M, Staines M, Long N J and Amemiya N 2018 AC loss characteristics in REBCO coil assemblies with different geometries and conductors *IEEE Trans. Appl. Supercond.* **28** 4700105

[23] Yamafuji K and Kiss T 1996 A new interpretation of the glass-liquid transition of pinned fluxoids in high-T_c superconductors *Physica* C **258** 197–212

[24] Kiss T *et al* 2003 Critical current properties in HTS tapes *Physica* C **392–396** 1053–62

[25] Higashikawa K, Kiss T, Inoue M, Awaji S, Watanabe K, Fukushima H, Yamada Y and Shiohara Y 2009 Significant reduction in volume, stored energy and magnetization loss of high-field magnet coil based on the improvement of critical current characteristics in GdBCO coated conductor *Physica* C **469** 1776–80

[26] Kiss T *et al* 2002 Angular dependence of critical current properties in YBCO coated tape under high magnetic field up to 18T *Physica* C **378–381** 1113–17

[27] Manfreda G 2011. Review of ROXIE's material properties database for quench simulations. *CERN Internal Note 2011-24 EDMS Nr:1178007*

[28] Willson M 1983 *Superconducting Magnets* (Oxford: Clarendon) pp 174–81

[29] Funaki K and Sumiyoshi F 1995 *Tashinsen to Doutai* (Tokyo: Sangyo Tosho) 34–35 (in Japanese)

[30] Brandt E H and Indenbom M 1993 Type-II superconductor strip with current in a perpendicular magnetic field *Phys. Rev.* B **48** 12893–906